The mixing layer and its coherence examined from the point of view of two-dimensional turbulence

By MARCEL LESIEUR, CHANTAL STAQUET,
PASCAL LE ROY AND PIERRE COMTE

Institut de Mécanique, Institut National Polytechnique de Grenoble and Université Scientifique
et Médicale, BP 68, 38402 Saint-Martin d'Hères, France

A two-dimensional numerical large-eddy simulation of a temporal mixing layer submitted to a white-noise perturbation is performed. It is shown that the first pairing of vortices having the same sign is responsible for the formation of a continuous spatial longitudinal energy spectrum of slope between k^{-4} and k^{-3}. After two successive pairings this spectral range extends to more than 1 decade. The vorticity thickness, averaged over several calculations differing by the initial white-noise realization, is shown to grow linearly, and eventually saturates. This saturation is associated with the finite size of the computational domain.

We then examine the predictability of the mixing layer, considering the growth of decorrelation between pairs of flows differing slightly at the first roll-up. The inverse cascade of error through the kinetic energy spectrum is displayed. The error rate is shown to grow exponentially, and saturates together with the levelling-off of the vorticity thickness growth. Extrapolation of these results leads to the conclusion that, in an infinite domain, the two fields would become completely decorrelated. It turns out that the two-dimensional mixing layer is an example of flow that is unpredictable and possesses a broadband kinetic energy spectrum, though composed mainly of spatially coherent structures.

It is finally shown how this two-dimensional predictability analysis can be associated with the growth of a particular spanwise perturbation developing on a Kelvin–Helmholtz billow: this is done in the framework of a one-mode spectral truncation in the spanwise direction. Within this analogy, the loss of two-dimensional predictability would correspond to a return to three-dimensionality and a loss of coherence. We indicate also how a new coherent structure could then be recreated, using an eddy-viscosity assumption and the linear instability of the mean inflexional shear.

1. Introduction

The mixing layer between two flows of velocities U_1 and U_2 has been extensively investigated experimentally over the last 15 years: in particular Brown & Roshko (1974) showed the persistence far downstream of large structures (usually called 'coherent') upon which small-scale three-dimensional turbulence is superposed, and Winant & Browand (1974) observed the pairing of these structures. An extensive review of the subject has been given by Ho & Huerre (1984). Mixing layers are encountered in aerodynamics, in the atmosphere or the ocean (e.g. in the wake of mountains, in the Gulf Stream or in the Mediterranean sea), as well as in the atmospheres of Jupiter and Saturn (at the interface between neighbouring zonal

jets). Such a flow permits the study of transition to turbulence far from boundaries. The concept of coherence applied to the large structures is somewhat controversial (see e.g. Wood & Bradshaw 1982). Other important questions are the relevance of the two-dimensional Navier–Stokes or Euler equations to describe properly the large quasi-two-dimensional scales, and how the latter interact with small-scale three-dimensional turbulence. In this paper, we shall examine the dynamics of the large scales of the mixing layer from the point of view of two-dimensional turbulence and of predictability theory, using numerical simulations.

In §2, numerical large-eddy simulations of the two-dimensional Navier–Stokes equations applied to the temporal mixing layer are presented; this type of calculation is not new (except for the higher spatial resolution employed here) and follows the work of Zabusky & Deem (1971), Couët & Leonard (1980), Riley & Metcalfe (1980), Aref & Siggia (1980), Cain, Reynolds & Ferziger (1981) and Corcos & Sherman (1984). In the present work, we introduce to the initial condition a small white-noise perturbation, in order to model (in a very rough way of course) the residual turbulence existing upstream in the unperturbed mixing-layer experiments. We shall focus on the longitudinal spatial spectral statistics of the flow associated with events occurring in the layer (i.e. growth of fundamental eddies and pairings). The latter are visualized by computer pictures displaying the vorticity field. We shall also compare these statistics with the predictions for homogeneous isotropic two-dimensional turbulence, and discuss the possibility for the mixing-layer coherent structures to be considered as a special case of two-dimensional turbulence.

In §3, we analyse the predictability of the mixing layer, looking at the growth of decorrelation between two flows differing initially by the white-noise perturbation only.

In §4, it is shown how a spanwise one-mode truncation of the three-dimensional mixing layer, consisting of a two-dimensional basic flow on which is superposed a sine-wave perturbation in the spanwise direction, is equivalent to the two-dimensional predictability problem. We discuss also possible mechanisms of destruction and recreation of the coherent structures, using both the former unpredictability results as well as linear instability arguments.

2. Two-dimensional large-eddy simulations

2.1. *Equations and numerical model*

Consider a two-dimensional incompressible flow with a stream function $\psi(x, y, t)$ satisfying the two-dimensional Navier–Stokes equation

$$\left[\frac{\partial}{\partial t} + J(\,.\,,\psi)\right]\nabla^2\psi = \nu\nabla^2(\nabla^2\psi),\qquad(2.1)$$

where $J(A, B)$ is the Jacobian operator $(\partial A/\partial x)(\partial B/\partial y) - (\partial A/\partial y)(\partial B/\partial x)$, and x, y, and z are respectively the streamwise, transverse and spanwise directions. Since we are mainly interested in a simulation of the large scales, the molecular viscous dissipative operator on the right-hand side of (2.1) will be replaced by a subgrid-scale dissipative term $-\nu_1(\nabla^2)^3\psi$, so that

$$\left[\frac{\partial}{\partial t} + J(\,.\,,\psi)\right]\nabla^2\psi = -\nu_1\nabla^4(\nabla^2\psi).\qquad(2.2)$$

This type of biharmonic dissipation is often used by oceanographers (see e.g. Holland 1978). Its utilization is of course open to debate, but it seems to allow a good description of the large scales of the flow, with dissipative effects shifted to the cutoff scale. It permits an artificial increase in the Reynolds number, and is consistent with a widely accepted point of view that, in high-Reynolds-number two-dimensional turbulence, the large scales are nearly inviscid, while the small scales dissipate vorticity fluctuations at a finite rate, as proposed by Batchelor (1969). It is not our aim here to investigate the validity of this subgrid-scale approximation for the mixing layer. This has been done by Basdevant & Sadourny (1983) in the case of homogeneous two-dimensional turbulence.

We have carried out a second-order, finite-difference numerical simulation of (2.2). The Jacobian terms are evaluated using Arakawa's (1966) formulation which conserves total kinetic energy and enstrophy and maintains the property

$$J(\nabla^2\psi, \psi) = -J(\psi, \nabla^2\psi).$$

The dissipative term always lags by one time-step to avoid (linear) numerical instability. Using a second-order leapfrog technique for the time differencing, with an occasional Euler forward time-stepping to eliminate time splitting of the calculated solutions, the numerical calculation finally reduces to solving a Poisson equation. This is done using a standard code written by Schwarztrauber & Sweet (1980), which allows various boundary conditions. In most of the calculations presented below, the stream function is defined on a regular array of 256^2 grid points with a uniform spacing in each direction.

We consider a 'temporal' mixing layer, i.e. with periodic boundary conditions in the x-direction. The calculation is carried out in a square domain of size D_N (the physical significance of D_N will be specified later). On $y = \pm\frac{1}{2}D_N$, we employ free-slip boundary conditions $\psi = 0$ and $\nabla^2\psi = 0$.

The velocity distribution of the basic flow at $t = 0$ is a hyperbolic tangent velocity profile $u(y) = U \tanh 2y/\delta_i$; x, y and t are made non-dimensional with respect to the velocity U and the initial vorticity thickness δ_i. The vorticity thickness $\delta(t)$ at any time is defined by $\delta = 2U/(d\bar{u}/dy)_{max}$, the bar denoting an average in the x-direction. The initial 'Reynolds number' based on these scales and characterizing the ratio of inertial to dissipative forces in (2.2) is $Re = U\delta_i^3/\nu_1$ and all the simulations are carried out at $Re = 10\,000$.

Superimposed upon the basic flow is a white-noise stream-function perturbation of small amplitude multiplied by $\exp(-y^2/\delta_i^2)$. This random perturbation injects energy into all the longitudinal spatial modes, and should reasonably approximate the case of a real mixing layer that is naturally submitted to a residual turbulence having a broadband spectrum. In that sense, the following calculations are closer to a real mixing layer than calculations with only deterministic perturbations.

It is known from linear stability analysis (Betchov & Szewczyk 1963) that perturbations corresponding to unstable modes will develop, since perturbations at all wavenumbers are initially present. The structures corresponding to the most amplified wavenumber (i.e. with the highest amplification rate) will appear first, corresponding to what we shall call a 'fundamental' mode. The associated most unstable wavelength λ_a given by the theory is approximately $\lambda_a = 7\delta_i$ (the most amplified wavenumber $2\pi/\lambda_a$ being $0.8892\ \delta_i^{-1}$, see Michalke 1964). Thus the side of the computational domain has to be taken equal to $D_N = 7N\delta_i$ in order to obtain N Kelvin–Helmholtz vortices in the streamwise direction: this is what we shall call an

'*N*-eddy calculation'. A further deterministic sine perturbation of wavelength λ_a and of small amplitude (modulated by the same Gaussian y-filter) is also superposed on the basic flow in order to fix the position (phase) of the Kelvin–Helmholtz eddies on the x-axis: without such a deterministic perturbation, the eddies would have, from one run to another, a randomly distributed position on this axis. In all the calculations that follow, U and the initial vorticity thickness δ_i will be the same, as will the deterministic sine perturbation, and the statistics of the various white-noise perturbations considered. The amplitudes of the two initial stream-function perturbations (random and deterministic) relative to the stream function of the mean flow are 10^{-3}. The calculations will differ in the number of eddies involved (and so the size D_N of the domain), the particular realizations of the white noise, and the number of grid points. For example, figure 1 (plate 1) shows a 4-eddy calculation (resolution 256^2) at time $t = 15\delta_i/U$ when the four eddies have appeared. The colours indicate the (algebraic) value of the vorticity from the minimum (blue) to the maximum (red). The vorticity of the basic inflexional velocity profile is negative; hence the blue colour will correspond to regions of high vorticity magnitude $2U/\delta_i$, and the red colour to the outer irrotational flow. We recall that, from the basic equation (2.2), the initial vorticity field is convected by the motion and diffused by viscosity: thus the values of the vorticity magnitude at any time cannot exceed $2U/\delta_i$ (this condition is not, however, exactly fulfilled in the calculation, owing to the replacement of the viscous harmonic dissipation by a biharmonic dissipation).

We have checked that the vorticity thickness is of the order of $2\delta_i$ when the fundamental eddies have appeared. Note finally that since a subharmonic perturbation is also initially present in the white noise, the subharmonic instability analysed by Kelly (1967) will grow, resulting generally in a pairing between the fundamental vortices (Riley & Metcalfe 1980); we have observed such pairing in most of our simulations.

With this temporal mixing layer we shall later associate a spatial problem with two velocities U_1 and U_2 such that $U_1 - U_2 = 2U$; the distance downstream of the splitter plate will correspond to $\frac{1}{2}t(U_1 + U_2)$. This is justified only if the streamwise growth of the spatial layer over distances of the order of D_N is neglected. Nevertheless, the main results of the following calculations (temporal case) may prove to be applicable in the spatial case also. Figure 2(a) (plate 2) shows an artificial spatial mixing layer associated with a calculation involving initially 8 eddies and reconstructed with 15 vorticity fields, separated by a period of time of $5\delta_i/U$. Figure 2(b) shows 9 vorticity fields displayed from $t = 0$ to $t = 80\delta_i/U$ in the 4-eddy calculation: this clearly exhibits the appearance of the fundamental structures as well as the first and the second pairing.

2.2. *Kinetic energy spectra*

A study of the mixing layer from the point of view of turbulence theories requires the calculation of statistical quantities, such as spectra. Since the mixing layer considered here is periodic in the x-direction only, the flow can be assumed statistically homogeneous only in this direction. Spatial Fourier transforms in the x-direction may therefore be considered; analogous Fourier transforms in the y-direction would be less significant physically since there is no periodicity in that direction. We consider then the one-dimensional longitudinal spectrum of the streamwise velocity component u:

$$E_1(k_x) = \frac{1}{2d} \int_{-d}^{+d} |\hat{u}(k_x, y)|^2 \, dy, \tag{2.3}$$
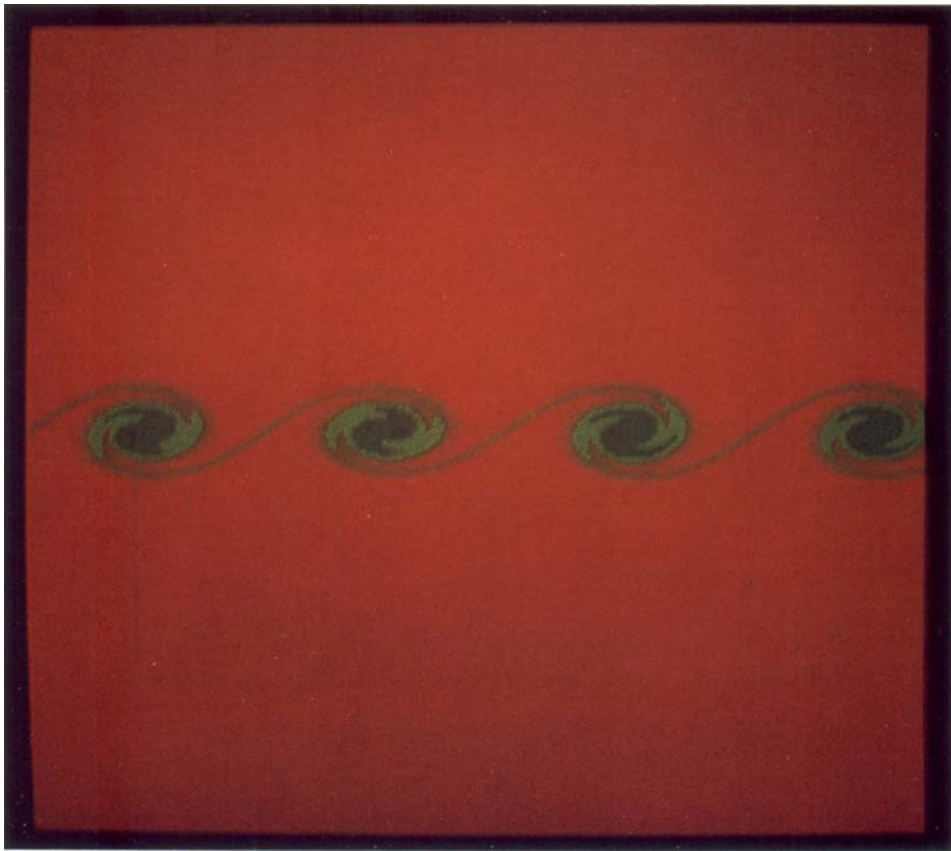
FIGURE 1. Vorticity field obtained after 15 characteristic initial turnover times δ_i/U in a 4-eddy calculation (256^2 grid points). Colours indicate the vorticity magnitude (blue for the regions of intense vorticity $2U/\delta_i$, red for the irrotational outer flow).
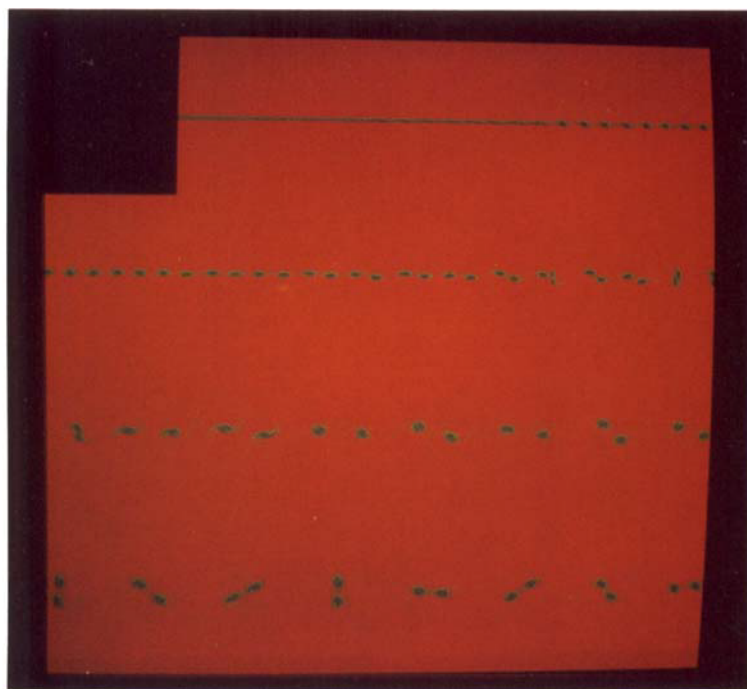
FIGURE 2. *(a)* Vorticity field of an artificial spatial mixing layer associated with the 8-eddy calculation (256^2 grid points). This field is obtained with a sequence of 15 vorticity fields separated by a period of time of $5\delta_1/U$. *(b)* 4-eddy calculation (256^2 grid points). The vorticity field is shown from $t = 0$ to $t = 80$.
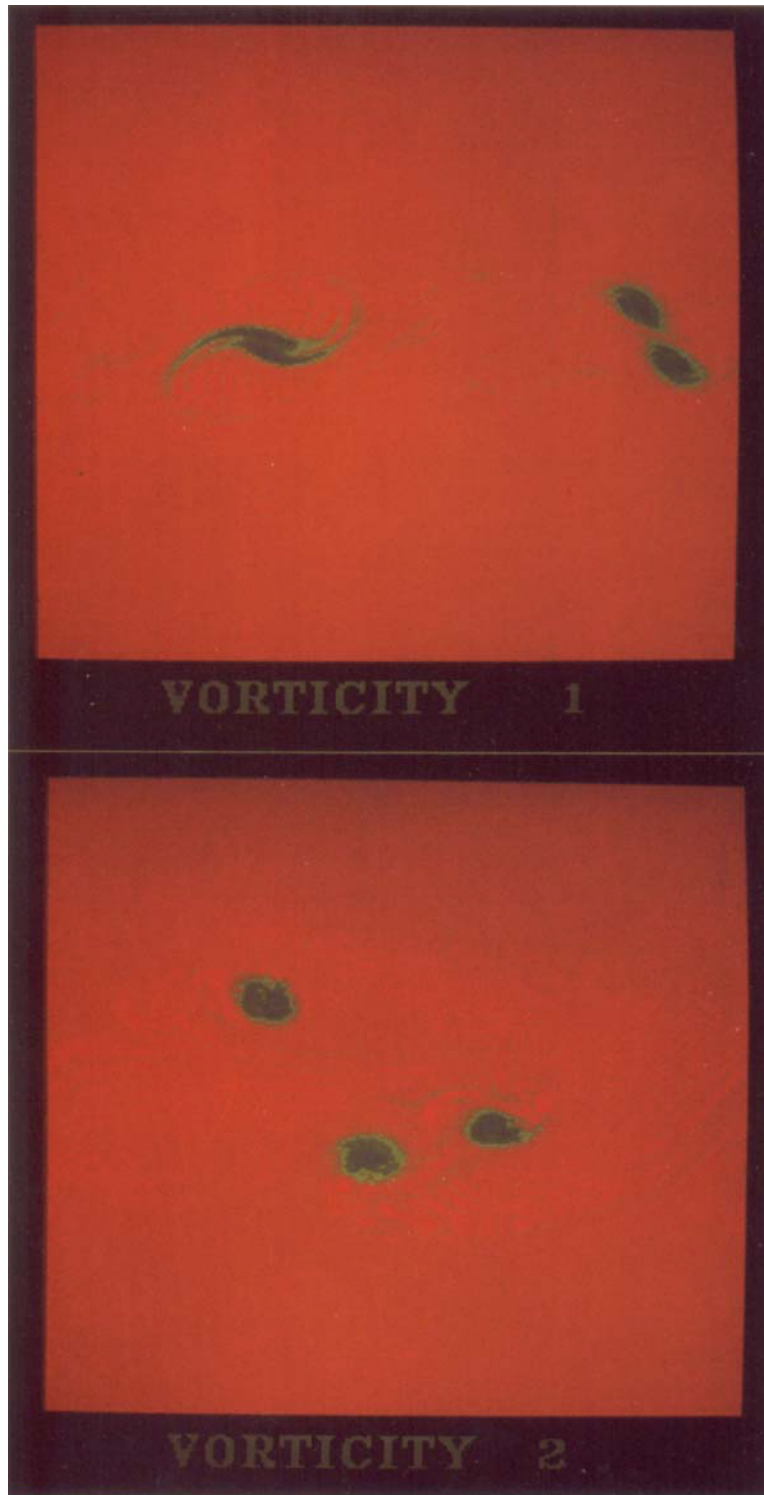
FIGURE 7. Sensitivity of the flow to the initial white noise (8-eddy calculation, 256^2 grid points). The vorticity field of the calculation of figure 5(b) is displayed at $t = 80$ for the two realizations of the initial white noise.

LESIEUR, STAQUET, LE ROY & COMTE

where $\hat{u}(k_x, y)$ is the longitudinal Fourier transform of the streamwise component u at a given y:

$$\hat{u}(k_x, y) = \frac{1}{D_N} \int_0^{D_N} u(x, y) \exp(-ik_x) x \, dx. \tag{2.4}$$

$2d \leqslant D_N$ corresponds to a y-span on which the logitudinal spectrum is averaged. The longitudinal wavenumber k_x will be restricted to positive values. One can also consider the longitudinal spectrum of the cross-stream velocity component v:

$$E_2(k_x) = \frac{1}{2d} \int_{-d}^{+d} |\hat{v}(k_x, y)|^2 \, dy, \tag{2.5}$$

with
$$\hat{v}(k_x, y) = \frac{1}{D_N} \int_0^{D_N} v(x, y) \exp(-ik_x) x \, dx. \tag{2.6}$$

For simplicity, k_x will hereinafter be denoted k. It must be stressed that if the two-dimensional turbulence were isotropic (which is obviously not the case for the mixing layer), the longitudinal energy spectrum $E_1(k_x)$ defined by (2.3) would be related to the isotropic energy spectrum $E(k)$ (integral of half the modal velocity variance $\frac{1}{2}|\hat{u}(k)|^2$ in Fourier space over a circular ring of radius $\approx k = |k|$) by the relation (see e.g. Mory & Hopfinger 1986; or Sommeria 1986)

$$E_1(k) = \frac{2}{\pi} \int_k^{+\infty} \frac{(p^2 - k^2)^{\frac{1}{2}}}{p^2} E(p) \, dp. \tag{2.7}$$

Then an inertial-range isotropic energy spectrum $E(k) \sim k^{-\alpha}$ will correspond to a $k_x^{-\alpha}$ longitudinal spectrum $E_1(k_x)$.

We present now the time evolution of a 4-eddy calculation in both physical and Fourier space: in figure 3 are plotted simultaneously the isovorticity lines of the velocity field and the one-dimensional longitudinal spatial energy spectrum $E_1(k)$ (defined from (2.3) with $d = \frac{1}{2}D_4$), for a calculation involving 183^2 grid points. The unit of time is δ_i/U. In figure 3(a) the small peak at the fundamental wavenumber $k_4 = 2\pi/\lambda_a$ corresponds to the small sine perturbation superposed upon the white noise (flat spectrum). At time $t = 20$ these eddies have been completely formed, and give rise to a peak in the energy spectrum (figure 3b). But nonlinear interactions between modes have already distributed the energy across a broad spectrum composed of two distinct parts: the harmonics of the fundamental mode k_4 emerge from the rest of the spectrum, where the pairing modes k_2 (first subharmonic $k_2 = \frac{1}{2}k_4$) and k_1 (second subharmonic $k_1 = \frac{1}{2}k_2$) begin to grow. At time $t = 40$, the first pairing is finished, and the two parts of the spectrum have collapsed into a k^{-4} range extending beyond k_2 (figure 3c). At time $t = 80$, at the end of the second pairing, the second subharmonic $k_1 = \pi/2\lambda_a$ has grown and increases the length of the k^{-4} range to 1.5 decades (figure 3d). In fact, the magnitude of the spectral exponent seems then to decrease slightly, perhaps towards the $-\frac{11}{3}$ value due to spiralling effects mentioned by Moffatt (1986).

We have also calculated in both cases the v-longitudinal energy spectra $E_2(k)$: they display the same behaviour as $E_1(k)$, that is, formation of a k^{-4} range after the first pairing. It is found that both u and v r.m.s. velocity fluctuations are of the same order in the calculation, which indicates that the turbulence at scales smaller than δ have some characteristics of two-dimensional isotropy. This is at variance with experimental mixing layers, where $v'^2 \approx w'^2 < u'^2$.

Figure 4 shows the time evolution of the kinetic energies of modes k_4, k_2 and k_1. The

(a)

(b)

(c)
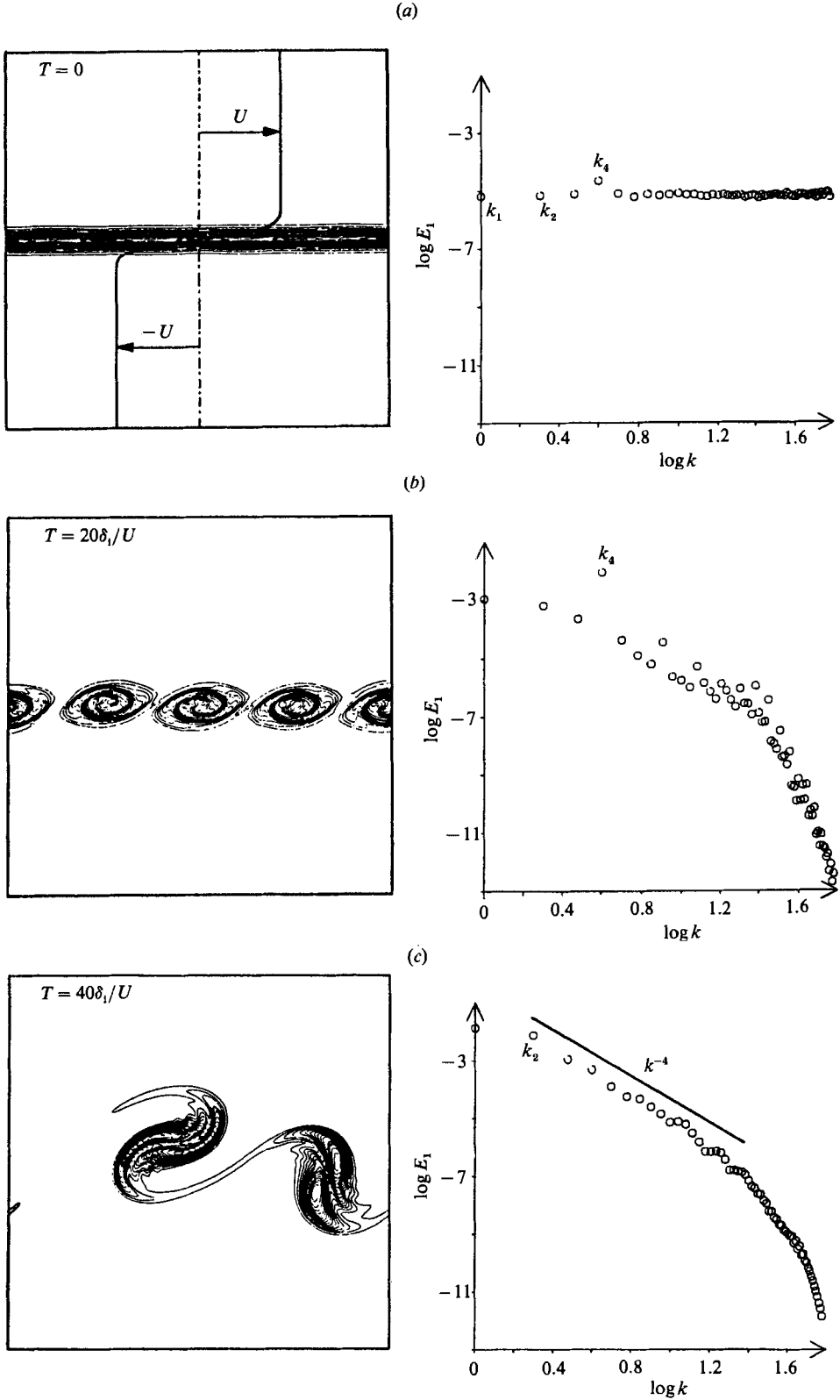
FIGURE 3(*a*, *b* and *c*). For caption see facing page.
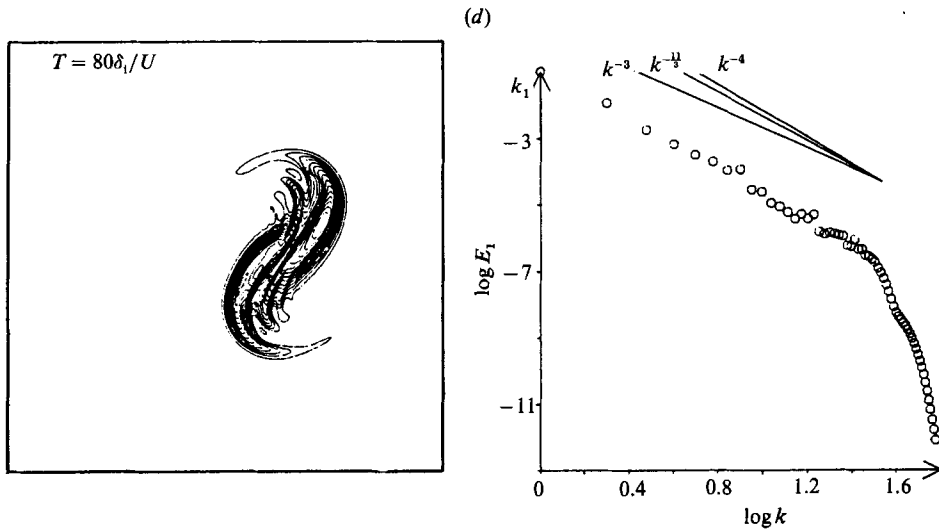
FIGURE 3. Isovorticity lines and corresponding spatial one-dimensional longitudinal energy spectra during the evolution of the mixing layer in a 4-eddy calculation (183^2 grid points). (*a*) The low-*k* cutoff wavenumber is $k_1 = 2\pi/4\lambda_a$. The wavenumber associated to the deterministic sine perturbation is $k_4 = 4k_1$. The flat spectrum corresponds to the white noise. (*b*) The fundamental mode grows. (*c*) End of the first pairing. (*d*) End of the second pairing.

formation of the coherent structures of wavelength λ_a and the first pairing are, respectively, associated with the maxima of $E_1(k_4)$ and $E_1(k_2)$ (at $t = 15$ and 35 respectively). The first maximum of $E_1(k_1)$ at $t = 50$ does not, as can be checked by the visualization of the vorticity fields in figure 2(*b*), correspond to the end of the second pairing, which actually occurs later, at about $t = 75$. This is due, as will be seen below, to an effect of the boundaries. The computing time (with this resolution of 183^2 grid points) for the emergence of the coherent structures and the two successive pairings is about 15 minutes on a CRAY 1 machine.

It is tempting to associate with the continuous spectrum we have found the words 'inertial range', used for isotropic two-dimensional turbulence. Furthermore the mechanism of the shearing of small-scale fluid elements by larger-scale velocity gradients, proposed to justify the enstrophy cascade concept (Kraichnan 1967; Leith 1968; Batchelor 1969), is certainly acting during the mixing-layer evolution. But the difference of our spectral exponent to the -3 value found in the classical enstrophy cascade statistical analysis is still an open question. A further analogy of the mixing layer with isotropic two-dimensional turbulence may be found in the large, spatially organized 'coherent structures' of the former, which resemble the coherent structures found by McWilliams (1984) in the isotropic case.

The fact that the two-dimensional mixing layer possesses a broad spatial spectrum and is, as will be seen in the next section, extremely sensitive to initial conditions and unpredictable, justifies considering it as a special case of two-dimensional turbulence (even though it is not isotropic). One might argue that in reality the spectra measured experimentally follow a $k^{-\frac{5}{3}}$ law at scales smaller than the vorticity thickness (Perry, Chong & Lim 1982; Browand & Ho 1983), and not the laws intermediate between k^{-4} and k^{-3} found in our simulations. This is due to the existence of small-scale three-dimensional turbulence whose Kolmogorov spectrum contaminates the 'coherent-structures spectrum' up to the large scales. However, it
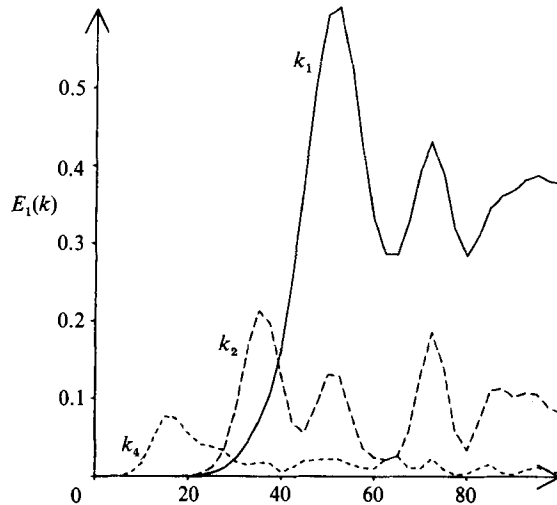
FIGURE 4. Evolution with time of the kinetic energy of the wavenumbers $k_1 = \pi/2\lambda_a$, $k_2 = 2k_1$ and $k_4 = 4k_1$, in the calculation of figure 3.

is likely that the large structures of the real three-dimensional mixing layer will retain in their memory the two-dimensional turbulent character exhibited in our numerical simulations. Thus, instead of denying the coherent structures the right of being called turbulent, we shall say, rather, that the turbulent mixing layer is composed of both two-dimensional (the coherent structures) and three-dimensional turbulence. Possible mechanisms of interaction between these two classes of turbulence will be examined in §4.

2.3. *Growth rate of the layer*

Figure 5 shows the evolution with time of the mean vorticity thickness $\delta(t)$, averaged over two realizations of the flow differing only in the initial white-noise perturbation. The calculations are all done with 256^2 grid points, and involve 4, 8 and 16 eddies (see figures 5a, b, c respectively). The size of the computational square is $D = D_4$, $2D = D_8$ and $4D = D_{16}$ in the cases a, b, c, respectively, with the same δ_i and deterministic perturbation in the three cases. Though the spatial resolution (number of grid points per fundamental eddy) decreases by a factor of 2 from (a) to (b) and from (b) to (c), the corresponding calculations and visualizations (cf. figures 2, 5b and 5c) tend to indicate that the loss of resolution does not change the essential dynamics of the layer. The advantage of these 8- and 16-eddy calculations compared with the 4-eddy case is, as will be seen, the possibility of further pairings without the constraining influence of the boundaries: on figure 5(a) are indicated the appearance of the fundamental eddies at $t = 15\delta_i/U$, the first pairing at $t = 35\delta_i/U$ and the second pairing at $t = 75\delta_i/U$. The figure also indicates clearly an inhibition of the layer spreading at about $t_B = 50\delta_i/U$, before the end of the second pairing. At times greater than 150, the smoothing observed on the curve corresponds to a single eddy having approximately a circular shape. On figure 5(b), where the domain width is twice as large, $t_B = 90\delta_i/U$ is subsequent to the second pairing. In figure 5(c), the influence of the boundaries starts at $t_B \approx 190\delta_i/U$, later than the third pairing. Figure 5(d), where the three calculations are superposed, summarizes these results and clearly indicates this boundary effect in the various calculations, and thus their

limit of validity (with respect to the free mixing layer in an infinite domain). It also shows that the mean slope of the linear growth in this temporal calculation is of the order of 0.10, smaller than the value of 0.17 found in various spatial mixing-layer experiments for the spreading constant $[(U_1+U_2)/(U_1-U_2)]\,\mathrm{d}\delta/\mathrm{d}x$ (see for example Liepmann & Laufer 1947, or Bernal 1981). It is not clear whether this difference is ascribable to the numerical techniques used, the two-dimensionality assumption or the temporal approximation itself. Notice however that the linear tendency of 0.10 obtained here comes from an averaging involving three successive pairings, but that the calculations show a quicker growth of the vorticity thickness up to the first pairing, more compatible with the spatial natural-mixing-layer experiments.

From the average tendency displayed above, a layer of thickness δ doubles its thickness in a time $\approx 10\delta/U$. Hence, it is possible to determine systematically the times at which the various pairings occur more precisely than with visual observations: if the fundamental eddies form at $t_1 = 15\delta_i/U$ (when the vorticity thickness is $2\delta_i$), the first pairing will occur at about

$$t_2 = t_1 + 10(2\delta_i/U) = 35\delta_i/U,$$

the second pairing at $\qquad t_3 = t_2 + 10(4\delta_i/U) = 75\delta_i/U,$

and the third pairing at $\qquad t_4 = t_3 + 10(8\delta_i/U) = 155\delta_i/U.$

For the associated spatial mixing layer, this would correspond to non-dimensional downstream distances $[(U_1-U_2)/(U_1+U_2)]\,(x/\delta_i)$ of 35, 75 and 155 for the first, second and third pairing, respectively. With the experimental spreading rate of 0.17, and taking the same time $t_1 = 15\delta_i/U$ for the formation of the fundamental eddies, one would obtain instead distances of 27, 50 and 97 for the three successive pairings. In the experiments of Ho & Huang (1982), the times of 28 and 56 are found for the first and the second pairing. Note that in figure 5(c) the strong decrease of the vorticity thickness at the end of the third pairing simply indicates a rotation of the eddies about each other. Note also that the times when the influence of the boundaries becomes noticeable correspond approximately to the end of the first pairing in the 4-eddy calculation and to the end of the second pairing in the 8-eddy calculation, when in both cases there remain two eddies in the computation domain. It is somewhat surprising that these two eddies can merge completely (as can be checked using the visualizations from the three cases a, b and c), without any further increase of the vorticity thickness (which increased regularly during the earlier pairings). We believed initially that this earlier saturation was due to the influence of the parallel boundaries $y = \pm D$. We then performed 8-eddy calculations in a rectangular domain of size $2D \times 4D$ (resolution 256×512), which do not show a significant increase in the vorticity-thickness amplitude, nor in the saturation time, compared with the corresponding calculation in the square domain. The saturation observed is therefore due to the periodicity in the x-direction, corresponding to the temporal approximation. Notice, however, that an 8-eddy calculation in a rectangular domain of size $2D \times D$ shows an influence of the parallel boundaries which slow down the growth of the vorticity thickness.

3. The predictability of the mixing layer

In general, the predictability problem in fluid dynamics consists in looking at the evolution of the separation between two flows initially very close. In this section we examine the predictability of the two-dimensional mixing layer, by considering two
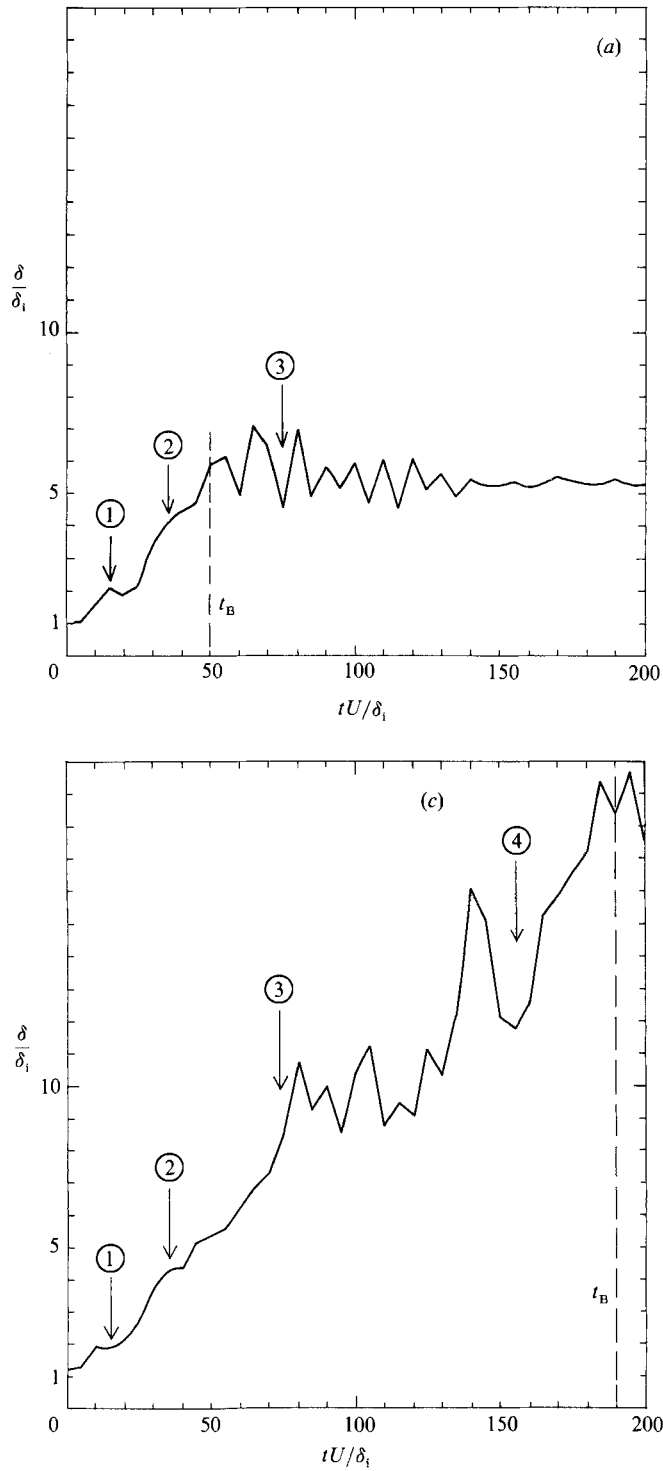
FIGURE 5 (*a* and *c*). For caption see facing page.
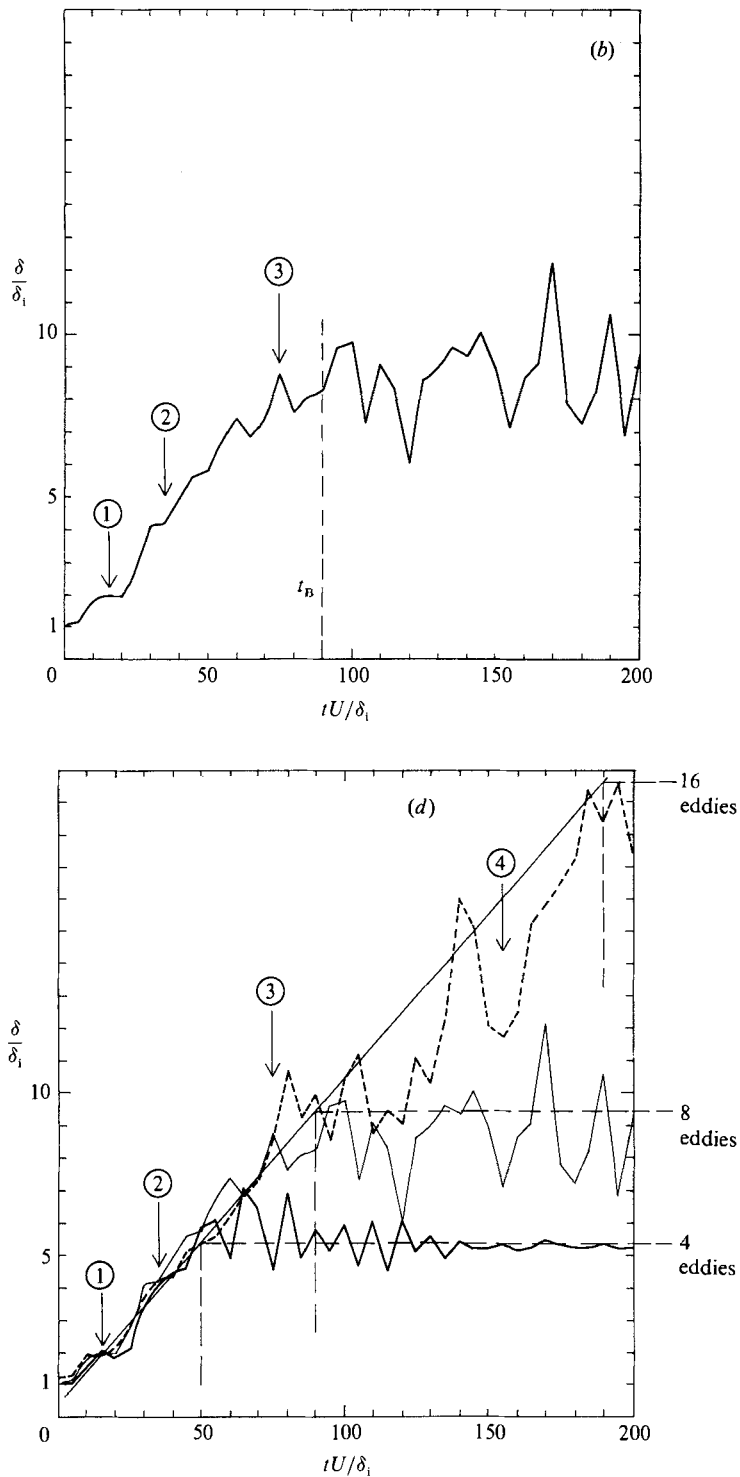
FIGURE 5. Evolution with time of the vorticity thickness averaged on two realizations of the flow differing only by the initial white-noise realization. Calculations (256^2 grid points) are carried out in a square domain of size: (a) D, (b) $2D$ and (c) $4D$ respectively. Arrows $1, 2, 3, 4$ indicate the fundamental structures formation and the first, second and third pairing respectively. t_B marks the layer growth inhibition due to the boundary conditions. On (d) the three calculations are superposed. The straight line shows the slope of the mean linear growth (0.10).

velocity fields $u_1(x, y, t)$ and $u_2(x, y, t)$ which evolve independently (in the same square domain D_N and with the same boundary conditions as in §2) according to the modified two-dimensional Navier–Stokes equation (22), with different initial conditions. Let

$$E_\Delta = \tfrac{1}{4}\langle[u_1(x, y, t) - u_2(x, y, t)]^2\rangle$$

$$= \frac{1}{8dD_N}\int_{-d}^{+d}\mathrm{d}y\int_0^{D_N}[u_1(x, y, t) - u_2(x, y, t)]^2\,\mathrm{d}x \qquad (3.1)$$

(where $u_1 - u_2$ is the longitudinal component of the velocity difference $\boldsymbol{u}_1 - \boldsymbol{u}_2$) be a spatial average of the longitudinal 'velocity difference energy' (hereinafter called error energy) in a rectangular test domain $x \in [0, D_N], y \in [-d, +d]$, with $2d = D = D_4$. Also, let

$$E_{2\mathrm{D}} = \tfrac{1}{2}\langle u_1^2\rangle = \frac{1}{4dD_N}\int_{-d}^{+d}\mathrm{d}y\int_0^{D_N}u_1^2(x, y, t)\,\mathrm{d}x \qquad (3.2)$$

(where u_1 is the longitudinal component of $\boldsymbol{u}_1$) characterize a mean two-dimensional kinetic energy. Such a choice allows the ratio

$$r(t) = \frac{E_\Delta}{E_{2\mathrm{D}}} \qquad (3.3)$$

to be zero if $\boldsymbol{u}_1 \equiv \boldsymbol{u}_2$, and equal to 1 if $\boldsymbol{u}_1$ and $\boldsymbol{u}_2$ are completely spatially decorrelated in the test domain. Also, we define the longitudinal error spectrum as

$$E_\Delta(k_x, t) = \frac{1}{2d}\int_{-d}^{+d}|\hat{u}_1(k_x, y, t) - \hat{u}_2(k_x, y, t)|^2\,\mathrm{d}y, \qquad (3.4)$$

with

$$\hat{u}_1(k_x, y, t) - \hat{u}_2(k_x, y, t) = \frac{1}{D_N}\int_0^{D_N}[u_1(x, y, t) - u_2(x, y, t)]\exp(-\mathrm{i}k_x)\,x\,\mathrm{d}x. \qquad (3.5)$$

In the case of isotropic two-dimensional turbulence, the Eddy-Damped Quasi-Normal Markovian (EDQNM) theory (or nearly equivalent Test-Field-Model) was applied to this statistical predictability problem by Leith & Kraichnan (1972) in the case of a stationary enstrophy cascade: they found that, for an error initially confined to large wavenumbers (but not in the dissipation range), the error rate $r(t)$ increases exponentially. The same study was carried out by Métais, Chollet & Lesieur (1983) and Métais & Lesieur (1986), both in the forced and decaying case. They showed that the initial large k error was very rapidly transferred to the energy-containing eddies of wavenumber k_i, owing to non-local interactions in Fourier space. In the problem where the error is initially injected in the 'energetic' wavenumbers $k_i(t_0)$, the results suggested that

$$r(t) \sim \exp[(t - t_0)/\sigma\tau_0], \qquad (3.6)$$

where τ_0 is the initial large-eddy turnover time when the error is injected into the system. σ is equal to 2.6 in the forced case and to 3.8 in the unforced case.

This result of exponential error growth is based on statistical closures of two-dimensional turbulence whose validity has often been questioned. Furthermore, and even if it were valid, its relevance for the mixing layer (which is neither isotropic nor even homogeneous) should be treated with caution. It is therefore useful to recover the
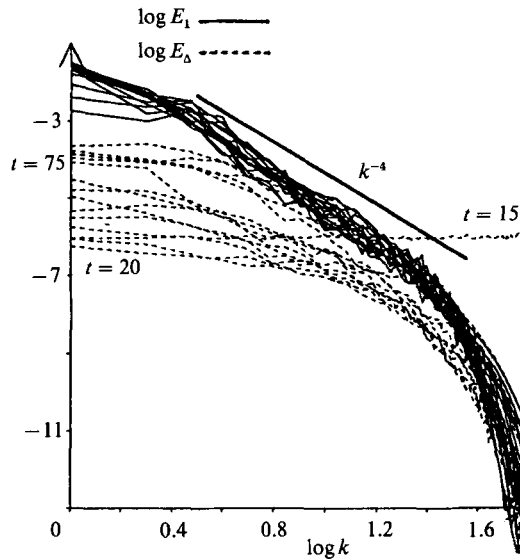
FIGURE 6. Kinetic energy and error spectra in the mixing layer (4-eddy calculation, 183^2 grid points). The initial error (white noise) has been superposed (at $t = 15$) on fundamental structures already formed. The error rises progressively in the large scales of the energy spectrum.

same kind of result (i.e. growth of decorrelation between two initially close realizations u_1 and u_2 of the flow) on the basis of the present numerical large-eddy simulation. Such a study was initiated by Staquet (1985) by perturbing with white noise a 4-eddy mixing layer once the fundamental eddies had been formed, and looking at the difference between the unperturbed and perturbed flow: in such a calculation the error rate, after a strong initial decrease, rose exponentially up to a value of about 0.05, then saturated for times greater than about 50 (which is precisely the time where the 4-eddy layer stops growing, owing to the boundary effect). Figure 6 shows the time evolution of the one-dimensional longitudinal error spectrum corresponding to Staquet's (1985) calculation: after a decay due both to the viscous dissipation and to the rather unrealistic initial perturbed flow u_2, an inverse cascade of error through the energy spectrum is observed. This is qualitatively similar to that observed by Leith & Kraichnan (1972) or Métais & Lesieur (1986) in the isotropic case.

Here, we have chosen to make the two fields $u_1(x, y, t)$ and $u_2(x, y, t)$ differ only in the initial (at $t = 0$) white noise, while having the same sine-wave perturbation at the most amplified mode, as in the calculations presented in figure 5: they will then develop the fundamental structures at the same x-location, and will thus (at $t = 15\delta_i/U$) differ by an error (due to the initial difference in the white noise) that will have had time to adjust to the equations. One can then study the evolution of the error $(u_1 - u_2)$ on the basis of a physically acceptable velocity field. As an example, figure 7 (plate 3) compares the two realizations of the mixing layer in the calculation of figure 5(b) at $t = 80$: significant differences are visible! The vorticity field 2 in figure 7 displays an 'anomalous pairing', where one eddy which was about to pair with its neighbour has suddenly changed its partner and will finally pair with the third eddy, as we have checked in the following sequences.

We then evaluated the error rate in the three cases studied in figure 5, calculating the error between the two fields for a square domain of side $D_4 = D$, $D_8 = 2D$, and
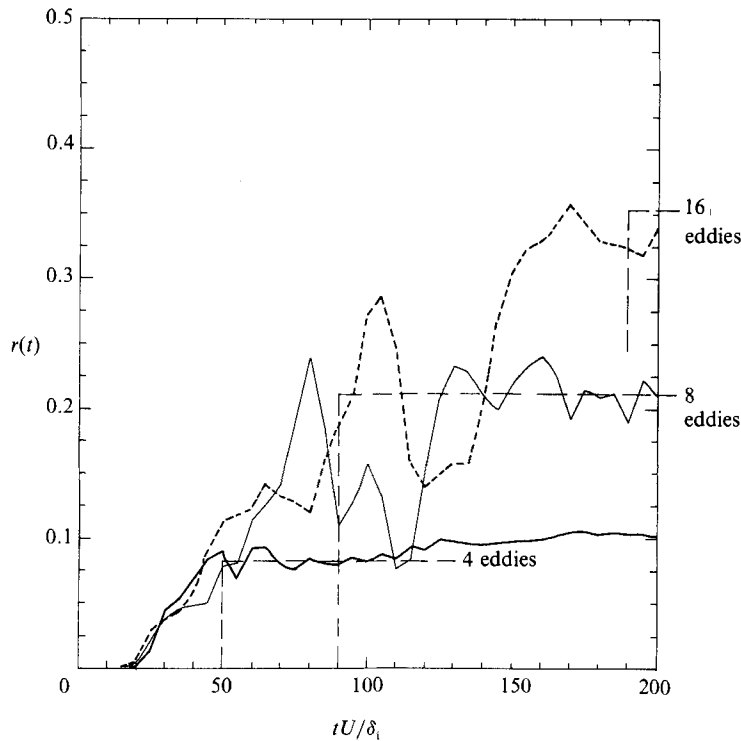
FIGURE 8. Evolution of the relative error rate averaged across the layer from $y = -\frac{1}{2}D$ to $y = +\frac{1}{2}D$ in the same calculation as in figure 5. The error stops increasing in the mean at the same time t_B (50, 90 and 150 respectively) as the layer stops growing.

$D_{16} = 4D$. For each case the error rate is calculated using (3.1), (3.2) and (3.3). This allows significant comparisons between the three cases studied: indeed, the initial deterministic conditions in the cases D_8 and D_{16} are obtained from those for D_4 by a translation of period D in the x-direction; as for the initial white-noise perturbation, its statistics in the streamwise direction are independent of D_N in (3.1) and (3.2). Thus, the initial value $r(0)$ is the same for the three cases, as found in the calculations.

The error rate $r(t)$, given by (3.3), is characteristic of the error energy, since E_{2D} given by (3.2) remains very close to its initial value, $O(U^2)$, given by the hyperbolic tangent velocity profile of the basic flow. $r(t)$ is presented on figures 8 and 9. Figure 8 clearly shows that the saturation of the error occurs at the same time t_B as the vorticity thickness stops growing, and is thus an effect of the finiteness of the domain and of the longitudinal periodicity: for instance the maximum value of the error rate rises from 0.1 to 0.35 when the size of the domain goes from D (4 eddies) to $4D$ (16 eddies). A calculation carried out in an infinite domain would presumably yield a further growth of $r(t)$ up to the maximum value of 1. The fluctuations observed in r are due both to the global rotation of the large structures, and to the fact that only the error between two realizations is calculated here, though the statistical predictability theory strictly requires an average over an ensemble of pairs of realizations: such an averaging would have been too costly, since the calculation of a single flow realization up to $t = 200\delta_i/U$ with 256^2 grid points already required 2.40 hours on the Grenoble University FPS 264 computer (and 7.40 hours for 256×512
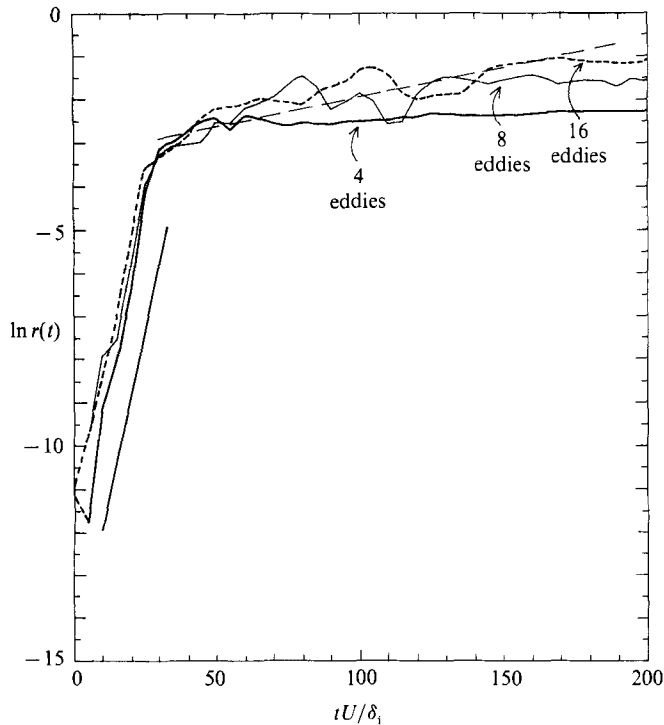
FIGURE 9. Same data as in figure 8, in semi-log coordinates; the error starts increasing exponentially with a characteristic time of $3\delta_i/U$ (straight line), up to $t = 25\delta_i/U$. Afterwards it still grows exponentially in the mean, with a characteristic time of $15\delta/U$, where δ is the vorticity thickness at the beginning of this period.

points). In figure 9 the same error rate is shown in semi-log coordinates for the three runs, and displays two distinct types of exponential behaviour: up to $t = 25\delta_i/U$, the error rate varies as

$$r(t) = r(0) \exp\left(\frac{Ut}{3\delta_i}\right). \tag{3.7}$$

This rapid increase corresponds to the formation of the fundamental eddies and the beginning of the first pairing, but leads to small values (0.05), because of the infinitesimal initial errors in our calculation. Then, after the first pairing (for $t > t_0 = 40\delta_i/U$), a second exponential phase follows, approximately described as

$$r(t) = r(t_0) \exp\left(\frac{U(t-t_0)}{15\delta(t_0)}\right). \tag{3.8}$$

Extrapolation of this law for an infinite domain would yield $r(t) = 1$ at $t = 240\delta_i/U$, and hence a complete decorrelation. Notice also in figure 9 a drastic change in the evolution of the error, which occurs during the first pairing but keeps on increasing thereafter until it saturates due to the x-periodicity: practically, one can say that the error grows as far as the layer thickness (measured by the vorticity thickness or the momentum thickness) increases.

Thus the temporal mixing layer excited initially with the aid of a tiny white-noise perturbation proves to be unpredictable, even though it is made of spatially coherent structures. This result indicates that the concepts of unpredictability and coherence are far from being contradictory.

4. The interaction between two- and three-dimensional turbulence

4.1. *From two- to three-dimensional turbulence*

Three-dimensional spanwise instabilities developing on Kelvin–Helmholtz billows have been studied experimentally by Bernal (1981), Jimenez (1983), Jimenez, Cogollos & Bernal (1985) or Lasheras, Cho & Maxworthy (1986) for instance. The results show essentially the development of a wave-like oscillation of the billows in the spanwise direction, with longitudinal pairs of counter-rotating vortices developing on the crests. Pierrehumbert & Widnall (1982) performed a theoretical linear stability analysis on Stuart vortices, which showed in particular that a spanwise sine-wave perturbation amplifies, with a most unstable wavelength of the order of $\frac{2}{3}\lambda_a$. Corcos & Lin (1984) generalized the latter study to an arbitrary time-evolving basic flow: they found basically the same result, and stressed also the role of the two-dimensional subharmonic mode (responsible for the pairing) as an inhibitor of the three-dimensionality development. Metcalfe *et al.* (1987) performed a three-dimensional direct numerical simulation showing the appearance of the longitudinal counter-rotating vortices, and confirming Corcos & Lin's predictions concerning the role of the subharmonic mode.

Here we shall develop a formalism showing an equivalence between a one-mode spanwise truncation of the three-dimensional mixing layer and the two-dimensional predictability problem studied above. Consider the following flow, where the velocity and pressure fields $u(x, t)$ and $p(x, t)$ are expanded as

$$u(x, y, z, t) = u_{2D}(x, y, t) + \sqrt{2}\, u_{3D}(x, y, t) \sin k_z z, \qquad (4.1)$$

$$p(x, y, z, t) = p_{2D}(x, y, t) + \sqrt{2}\, p_{3D}(x, y, t) \sin k_z z, \qquad (4.2)$$

where u_{2D} and u_{3D} are parallel to the (x, y)-plane and non-divergent. These two fields represent, respectively, the basic two-dimensional flow and the amplitude of the three-dimensional perturbation; k_z is a constant. A schematic three-dimensional representation of the vorticity field is given in figure 10. Such a velocity field is non-divergent, since its z-component is zero. This decomposition parallels the analysis leading to the 'barotropic' and 'baroclinic' spectral two-mode decomposition of the quasi-geostrophic equation for rapidly rotating fluids (see e.g. Hoyer & Sadourny 1982), the latter being the equivalent of the quasi-geostrophic two-layer model (see e.g. Pedlosky 1979 for details). The essence of the one-mode spanwise truncation of the three-dimensional Navier–Stokes equation is to assume that the form (4.1), (4.2) is conserved with time, and to discard the fluctuations in the spanwise mode $2k_z$ which are produced by nonlinear interactions. Consider the three-dimensional Navier–Stokes equation (with constant density)

$$\frac{\partial u}{\partial t} + u \cdot \nabla u = -\nabla p + \nu \nabla^2 u, \qquad (4.3)$$

in which we substitute the particular expansions (4.1) and (4.2). One obtains

$$\begin{aligned}
&\frac{\partial u_{2D}}{\partial t} + u_{2D} \cdot \nabla u_{2D} + 2 \sin^2 k_z z \; u_{3D} \cdot \nabla u_{3D} \\
&\quad + \sqrt{2} \sin k_z z \left(\frac{\partial u_{3D}}{\partial t} + u_{2D} \cdot \nabla u_{3D} + u_{3D} \cdot \nabla u_{2D} \right) \\
&= -\nabla p_{2D} - \sqrt{2} \sin k_z z \, \nabla p_{3D} + \nu [\nabla^2 u_{2D} + \sqrt{2} \sin k_z z \, (\nabla^2 u_{3D} - k_z^2 u_{3D})]. \quad (4.4)
\end{aligned}$$
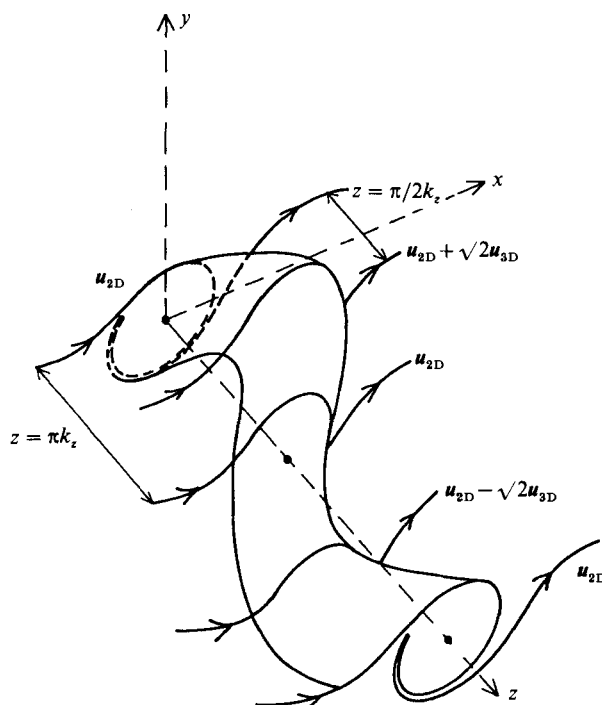
FIGURE 10. Schematic view of a three-dimensional instability of wave length $2\pi/k_z$ developing on a coherent structure.

Noticing that $2\sin^2 k_z z = 1 - \cos 2k_z z$, eliminating the $\cos 2k_z z$ term (which corresponds to the truncation), we obtain after identification of the $\sin k_z z$ terms

$$\frac{\partial \boldsymbol{u}_{2\mathrm{D}}}{\partial t} + \boldsymbol{u}_{2\mathrm{D}} \cdot \boldsymbol{\nabla} \boldsymbol{u}_{2\mathrm{D}} + \boldsymbol{u}_{3\mathrm{D}} \cdot \boldsymbol{\nabla} \boldsymbol{u}_{3\mathrm{D}} = -\boldsymbol{\nabla} p_{2\mathrm{D}} + \nu \nabla^2 \boldsymbol{u}_{2\mathrm{D}}, \tag{4.5}$$

$$\frac{\partial \boldsymbol{u}_{3\mathrm{D}}}{\partial t} + \boldsymbol{u}_{2\mathrm{D}} \cdot \boldsymbol{\nabla} \boldsymbol{u}_{3\mathrm{D}} + \boldsymbol{u}_{3\mathrm{D}} \cdot \boldsymbol{\nabla} \boldsymbol{u}_{2\mathrm{D}} = -\boldsymbol{\nabla} p_{3\mathrm{D}} + \nu \nabla^2 \boldsymbol{u}_{3\mathrm{D}}. \tag{4.6}$$

(In (4.6), the $\sim \nu k_z^2 \boldsymbol{u}_{3\mathrm{D}}$ term (arising in (4.4)) has been neglected in the dissipation term; we think this term would have only a negligible influence on the following results).

These equations present similarities with one of the cases (the 'coupled case') studied by Corcos & Lin (1984, see their equations 2.2b and 2.3), but in our model the $\boldsymbol{\nabla}$ operator is two-dimensional. Now let

$$\boldsymbol{u}_1(x, y, t) = \boldsymbol{u}_{2\mathrm{D}} + \boldsymbol{u}_{3\mathrm{D}}, \quad \boldsymbol{u}_2(x, y, t) = \boldsymbol{u}_{2\mathrm{D}} - \boldsymbol{u}_{3\mathrm{D}} \tag{4.7}$$

and similarly for p_1 and p_2. It is easy to show from (4.5) and (4.6) that $\boldsymbol{u}_1$ and $\boldsymbol{u}_2$ both satisfy independent two-dimensional Navier–Stokes equations, with the same boundary conditions as $\boldsymbol{u}(x, y, z, t)$ for $y = \pm\infty$. Therefore, the growth of this particular three-dimensional perturbation, if initially of random amplitude, can be expressed in terms of the predictability problem studied in the preceding section. Conversely, the study of $\frac{1}{2}(\boldsymbol{u}_1 - \boldsymbol{u}_2) = \boldsymbol{u}_{3\mathrm{D}}$ in the predictability problem will give access to the three-dimensional perturbation amplitude. E_Δ, given by (3.1), can then be

easily identified with the mean kinetic energy of the three-dimensional perturbation, averaged over a wavelength $2\pi/k_z$ in the spanwise direction. A value of 1 for $r(t)$ in (3.3) will then mean complete three-dimensionalization.

Such an analysis is of course subject to criticism, since there is no lateral velocity in the velocity field. The discarding of the $\cos 2k_z z$ term certainly eliminates some important three-dimensional characteristics of the flow, such as the existence of secondary streamwise vortices (Bernal 1981) or of small-scale three-dimensional turbulence. It has to be stressed that the streamwise secondary vortices found experimentally might just develop as a topological consequence of the spanwise oscillation of the Kelvin–Helmholtz billow described above, and hence a description of the flow focusing on only the spanwise oscillation might be of some relevance. On the other hand, the same truncation applied to the quasi-geostrophic potential vorticity equation yields valuable results regarding the baroclinic instability, which is nothing more than the growth of three-dimensionality in a quasi-two-dimensional eddy (with vertical axis) of the type presented in figure 10. But, as stressed by a referee, the rapid rotation in the quasi-geostrophic theory might eliminate precisely those stretching and tilting effects that we are studying, and render the decomposition valid in this case. At any rate, the present one-mode spanwise expansion provides a systematic formalism relating a wave-like tilting of the Kelvin–Helmholtz billows to the two-dimensional predictability. This gives a mathematical justification to, and sheds a new light on, an analogy already proposed by Lesieur (1983) and Staquet, Métais & Lesieur (1985), and discussed from the point of view of the statistical theory of turbulence by Métais & Lesieur (1986): within this formalism, the two fields u_1 and u_2 were two cross-sections of the flow in the (x, y)-plane at two distinct spanwise locations, which were assumed to be decorrelated. This could of course be valid only for spanwise wavelengths much longer than the vorticity thickness.

Owing to this mechanism, and using the predictability results of §3, we suggest that in an infinite domain (for a temporal layer), or in a spatial layer (where there is no periodicity constraint in the spatial direction), the initially quasi-two-dimensional layer would return exponentially to three-dimensionality. An estimate of the characteristic time of three-dimensionalization for a mixing layer of vorticity thickness $\delta(t_0)$, with Kelvin–Helmholtz billows formed and perturbed at $t = t_0$ by a three-dimensional perturbation of relative kinetic energy $r(t_0)$, is given by (3.8) with $r(t_0) = 1$. This yields

$$T_{3\mathrm{D}} = 15 \frac{\delta(t_0)}{U} \ln r(t_0)^{-1}. \tag{4.8}$$

Here, three-dimensionality does not mean *a priori* loss of spanwise coherence: but it is conceivable that once a Kelvin–Helmholtz billow has developed strong spanwise distortions, it may break down into developed three-dimensional turbulence with a $k^{-\frac{5}{3}}$ kinetic energy spectrum. It has to be stressed that our particular two-mode analysis has no preferred spanwise wavelength since all the spanwise perturbations have the same amplification rate, regardless of k_z. This is a further difference with respect to the analysis of Pierrehumbert & Widnall (1982) or Corcos & Lin (1984).

Experimentally, the three-dimensionalization of the layer is particularly spectacular in the initial stage of the evolution downstream of the splitter plate: the non-dimensional 'transition' distance D_{tr} found is (Jimenez 1983)

$$\frac{U_1 - U_2}{U_1 + U_2} \frac{D_{\mathrm{tr}}}{\delta_{\mathrm{i}}} \approx 60. \tag{4.9}$$

With the initial value $r(0) = 1.7 \times 10^{-5}$ taken in our calculations, the three-dimensionalization distance is of the order of 240, as already stressed. But it is clear from figure 9 that an initial value $r(0) = 1.2 \times 10^{-4}$ would yield $r(t) = 1$ at $t = 80$, closer to the value (4.9). It is thus difficult to predict theoretically the transition distance in the absence of experimental data concerning the amplitude of the three-dimensional turbulence immediately downstream of the splitter plate. It might be that the abrupt transition between (3.7) and (3.8) corresponds to the catastrophic occurrence of three-dimensionalization found experimentally in the initial stage. As for the law (4.8), it will apply in the 'developed region', downstream of D_{tr}.

Another important question concerns the role played by the two-dimensional subharmonic instability in the growth of spanwise instabilities: in our model, the mean three-dimensional kinetic energy still increases during the successive pairings, though much slower than during the initial stage (up to the first pairing). On the other hand, calculations of Corcos & Lin (1984) and Metcalfe *et al.* (1987) show a saturation in the growth of the three-dimensional kinetic energy, associated with the existence of a subharmonic pairing mode. But these calculations consider deterministic initial perturbations (contrary to our white-noise perturbations), consider only the first pairing, and might not involve domains and times large enough to eliminate the possibility of a further growth of three-dimensionality, after a slowing down during the first pairing. It seems, therefore, that three-dimensional calculations involving several pairings are needed in order to resolve this important question.

4.2. *From three- to two-dimensional turbulence*

Let us consider now the developed region of the mixing layer (after the transition to three-dimensional turbulence): several experiments (see e.g. Browand & Troutt 1980) have confirmed that the large coherent structures are still present far downstream, hidden behind the agitation of small-scale three-dimensional turbulence. We then assume that one of these large structures is perturbed by a spanwise oscillation and will, from the results of the last section, breakdown into three-dimensional turbulence. We now have a three-dimensional turbulent layer superposed upon a mean inflexional shear of vorticity thickness δ. For instance, as already mentioned, the longitudinal spectra determined by Browand & Ho (1983) in the central region of a high-Reynolds-number mixing layer show a nice $k^{-\frac{5}{3}}$ Kolmogorov cascade beyond the wavenumber δ^{-1} characteristic of the large scales, indicating that the mixing layer could be a superposition of coherent structures and of three-dimensional turbulence not far from isotropy. We assume then that the action of three-dimensional turbulence on the large coherent scales that are about to form can be modelled with the aid of an eddy viscosity ν_t, and that during the stage corresponding to the presence of small-scale turbulence superposed on the large-scale inflexional shear, one can write the equation

$$\left[\frac{\partial}{\partial t} + \mathrm{J}(\,.\,, \psi) \right] \nabla^2 \psi = \nu_t \nabla^2 (\nabla^2 \psi) \qquad (4.10)$$

where $\psi(x, y, t)$ is a stream function representing the two-dimensional large scales (mean shear + a two-dimensional broadband spectrum perturbation $\tilde{\psi}(x, y, t)$). The value of ν_t can be evaluated either by measuring experimentally the Reynolds stresses (Wygnanski & Fielder 1970), or by recourse to the concept of eddy viscosity in spectral space introduced by Kraichnan (1976) and used for large-eddy simulation by Chollet & Lesieur (1981) (see Lesieur 1987 for a review). In the latter case, and

when working in Fourier space, this eddy viscosity can be expressed in terms of the kinetic energy spectrum at the cutoff wavenumber k_C, and written

$$\nu_t = 0.28 \left[\frac{E(k_C)}{k_C} \right]^{\frac{1}{2}}. \tag{4.11}$$

For the mixing layer, we decide quite arbitrarily to consider that the large scales extend up to $k_C = 2\delta^{-1}$, and still assume that the action of modes $k > k_C$ upon the large scales correspond to the eddy viscosity (4.2) determined with the aid of energy spectra measured in the experiments (Lesieur 1983). This yields

$$\frac{\delta U}{\nu_t} = 30 \sim 40 \tag{4.12}$$

for the 'turbulent Reynolds number'. Then the perturbation $\tilde{\psi}$, which can initially be provided by the three-dimensional turbulence itself, will satisfy the Orr–Sommerfeld equation (but with the eddy viscosity replacing the molecular viscosity) and the most amplified coherent structure $\lambda_a = 7\delta$ will appear in a characteristic time $\approx 10 \sim 15\delta/U$: the coherent structure will then emerge from the smaller-scale turbulence. A similar behaviour has been observed experimentally (Browand & Ho 1983) when a mixing layer is forced across a grid in a wind tunnel. The role of the mean flow instability in the formation of the coherent structures had previously been pointed out by Taneda (1981).

Hence we suggest that the evolution of the mixing layer in the developed region and in an infinite domain is characterized by a cyclic exchange of energy between two- and three-dimensional turbulence: starting from a two-dimensional 'coherent structure' of vorticity thickness δ_0, spanwise decorrelation develops exponentially until it breaks down into three-dimensional turbulence and the coherence is lost. The characteristic time for such a destruction is still given by (4.8), but $r(t_0)$ is no longer very small, since the three-dimensional perturbation corresponds now to developed three-dimensional turbulence. Thus the characteristic time of destruction will be of the order of $15\delta(t_0)/U$. Then the ambient mean inflexional shear acts (through linear instability mechanisms) to build a new coherent structure. This is certainly an oversimplified view, compared with the complexity of various instabilities contributing to the three-dimensionalization or the coherence of the mixing layer, but it may nevertheless shed some light on the persistence far downstream of two-dimensional coherent structures. Let us remark finally that both mechanisms could occur simultaneously; as noted by J. J. Riley (1987, private communication).

5. Conclusion

This paper has studied the large coherent structures of a temporal mixing layer from a two-dimensional point of view. Large-eddy numerical simulations have shown that these structures, if excited initially by a white-noise perturbation superposed on a hyperbolic tangent basic velocity profile, are turbulent in the following sense: they are extremely sensitive to initial conditions ('unpredictable'), and they develop, after the first pairing, a broadband energy spectrum of slope intermediate between k^{-4} and k^{-3}. The mixing-layer vorticity-thickness growth is interrupted when the last two eddies merge, owing to the periodicity in the x-direction of the temporal approximation.

The predictability of the two-dimensional mixing layer has been investigated by

looking in particular at the growth of the error energy between two fields forced by the same perturbation at the fundamental mode, but differing initially in the white-noise perturbation realization. The error has been shown to grow exponentially, and saturates together with the vorticity thickness, owing to the same periodicity effect.

It has also been shown how a one-mode spanwise spectral expansion of the three-dimensional mixing layer is equivalent to a two-dimensional predictability problem, the kinetic energy of the wave-like spanwise perturbation being associated with the error energy betwen two independent two-dimensional fields.

Thus, the exponential loss of predictability mentioned above has been used to infer in the mixing layer an exponential growth of three-dimensionality induced by the particular spanwise perturbation considered above.

We have also proposed that, if the layer returns to three-dimensionality, a new coherent structure will then form, owing to the instability of the mean inflexional shear, upon which the three-dimensional turbulence would simply act as an eddy viscosity. Since the times for the destruction of the coherent structure depend logarithmically upon the amplitude of the initial perturbations, the exchange between 'coherence' (two-dimensional turbulence) and three-dimensional turbulence will be intermittent when the perturbations are randomly distributed in space.

A new image of the turbulent mixing layer can be proposed from these results: the mixing layer is a superposition of two-dimensional turbulence (the coherent structures, of spectrum intermediate between k^{-3} and k^{-4}), and three-dimensional turbulence close to isotropy and following approximately the Kolmogorov $k^{-\frac{5}{3}}$ law. These two states under which turbulence is condensed interact in two ways: first the exponential spanwise distortion of the Kelvin–Helmholtz billows cascades into small-scale three-dimensional turbulence. Secondly the linear instability of the mean inflexional shear, on which the three-dimensional turbulence serves both as an eddy viscosity and a perturbation, recreates two-dimensional Kelvin–Helmholtz billows.

A last point concerns the application of these concepts to other flows: some of the conclusions relating to three-dimensional instability growth may be applicable to large-Reynolds-number flows where large 'coherent' quasi-two-dimensional structures tend to be created by some instability mechanism, and compete with the development of three-dimensional turbulence, e.g. for wakes or jets, thermal convective flows at high Rayleigh numbers, and rotating flows such as Couette–Taylor flow or turbulence in a rotating tank (Hopfinger, Browand & Gagne 1982). In the last case, the analysis carried out in §4 for an eddy with axis parallel to the axis of solid-body rotation Ω in fact yields the same set of equations as (4.5) and (4.6), with Coriolis force contributions ($-2\Omega \times u_{2D}$ and $-2\Omega \times u_{3D}$ respectively) which are irrotational (provided Ω is a constant) and can therefore be included in the pressure terms. The same ideas of continuous destruction and recreation of the large organized structures may hold also for three-dimensional coherent structures, such as the 'hairpin' or 'horseshoe' vortices found in turbulent boundary layers (Kline *et al.* 1967; Taneda 1981; Head & Bandyopadhyay 1981; Moin & Kim 1982; Perry & Chong 1982); indeed they could result from the development of a sort of spanwise instability developing on two-dimensional eddies of a Tollmien–Schlichting type.

REFERENCES

ARAKAWA, A. 1966 Computational design for long-term numerical integration of the equations of fluid motion: two-dimensional incompressible flow. *J. Comp. Phys.* **1**, 119–143.

AREF, H. & SIGGIA, E. D. 1980 Vortex dynamics of the two-dimensional turbulent shear layer. *J. Fluid Mech.* **100**, 705–737.

BASDEVANT, C. & SADOURNY, R. 1983 Modeling of virtual scales in numerical simulation of two-dimensional turbulent flows. *J. Méc. Theor. Appl. Special Issue, Two-Dimensional Turbulence* (ed. R. Moreau), pp. 243–269.

BATCHELOR, G. K. 1969 Computation of the energy spectrum in homogeneous two-dimensional turbulence. *Phys. Fluids Suppl.* **II**, **12**, 233–239.

BERNAL, L. P. 1981 The coherent structure of turbulent mixing layers. Ph.D. thesis, California Institute of Technology, Pasadena.

BETCHOV, R. & SZEWCZYK, G. 1963 Stability of a shear layer between parallel streams. *Phys. Fluids* **6**, 1391–1396.

BROWAND, F. K. & HO, C. M. 1983 The mixing-layer: an example of quasi two-dimensional turbulence. *J. Méc. Theor. Appl., Special Issue, Two-Dimensional Turbulence* (ed. R. Moreau), pp. 99–120.

BROWAND, F. K. & TROUTT, T. R. 1980 A note on spanwise structure in the two-dimensional mixing layer. *J. Fluid Mech.* **93**, 325–336.

BROWN, G. L. & ROSHKO, A. 1974 On density effects and large structure in turbulent mixing layers. *J. Fluid Mech.* **64**, 775–816.

CAIN, A. B., REYNOLDS, W. C. & FERZIGER, J. H. 1981 A three-dimensional simulation of transition and early turbulence in a time-developing mixing layer. *Rep.* TF-14. Stanford, California.

CHOLLET, J. P. & LESIEUR, M. 1981 Parameterization of small scales of three-dimensional isotropic turbulence utilizing spectral closures. *J. Atmos. Sci.* **38**, 2747–2757.

CORCOS, G. M. & LIN, S. J. 1984 The mixing layer: deterministic models of a turbulent flow. Part 2. The origin of the three-dimensional motion. *J. Fluid Mech.* **139**, 67–95.

CORCOS, G. M. & SHERMAN, F. S. 1984 The mixing layer: deterministic models of a turbulent flow. Part 1. Introduction and the two-dimensional flow. *J. Fluid Mech.* **139**, 29–65.

COUËT, B. & LEONARD, A. 1980 Mixing layer simulation by an improved three-dimensional vortex-in-cell algorithm. In *Proc. 7th Intl Conf. on Numerical Methods in Fluid Dynamics.* Stanford-Ames.

HEAD, M. R. & BANDYOPADHYAY, P. 1981 New aspects of turbulent boundary layer structure. *J. Fluid Mech.* **107**, 297–337.

HO, C. M. & HUANG, L. S. 1982 Subharmonic and vortex merging in mixing layers. *J. Fluid Mech.* **119**, 443–473.

HO, C. M. & HUERRE, P. 1984 Perturbed free shear layers. *Ann. Rev. Fluid Mech.* **16**, 365–424.

HOLLAND, W. R. 1978 The role of mesoscale eddies in the general circulation of the ocean. *J. Phys. Oceanogr.* **8**, 363–392.

HOPFINGER, E. J., BROWAND, F. K. & GAGNE, Y. 1982 Turbulence and waves in a rotating tank. *J. Fluid Mech.* **125**, 505–534.

HOYER, J. M. & SADOURNY, R. 1982 Closure modeling of fully developed baroclinc instability. *J. Atmos. Sci.* **39**, 707–721.

JIMENEZ, J. 1983 A spanwise structure in the plane shear layer. *J. Fluid Mech.* **132**, 319–336.

JIMENEZ, J., COGOLLOS, M. & BERNAL, L. P. 1985 A perspective view of the plane mixing layer. *J. Fluid Mech.* **152**, 125–143.

KELLY, R. E. 1967 On the stability of an inviscid shear layer which is periodic in space and time. *J. Fluid Mech.* **27**, 657–689.

KLINE, S. J., REYNOLDS, W. C., SCHRAUB, F. A. & RUNSTADLER, P. W. 1967 The structure of turbulent boundary layers. *J. Fluid Mech.* **30**, 741–773.

KRAICHNAN, R. H. 1967 Inertial ranges in two-dimensional turbulence. *Phys. Fluids* **10**, 1417–1423.

KRAICHNAN, R. H. 1976 Eddy viscosity in two and three dimensions. *J. Atmos. Sci.* **33**, 1521–1536.

LASHERAS, J. C., CHO, J. S. & MAXWORTHY, T. 1986 On the origin and evolution of streamwise vortical structures in a plane, free shear layer. *J. Fluid Mech.* **172**, 231–258.

LEITH, C. E. 1968 Diffusion approximation for two-dimensional turbulence. *Phys. Fluids* **11**, 671–673.

LEITH, C. E. & KRAICHNAN, R. H. 1972 Predictability of turbulent flows. *J. Atmos. Sci.* **29**, 1041–1058.

LESIEUR, M. 1983 Intermittency of coherent structures, an approach using statistical theories of isotropic turbulence. In *Turbulence and Chaotic Phenomena in Fluids* (ed. T. Tatsumi), pp. 339–350. North-Holland.

LESIEUR, M. 1987 *Turbulence in Fluids*. Nijhoff.

LIEPMANN, H. W. & LAUFER, J. 1947 Investigation of free turbulent mixing. *NACA Tech. Note*, nx 1257.

McWILLIAMS, J. C. 1984 The emergence of isolated coherent vortices in turbulent flows. *J. Fluid Mech.* **146**, 21–43.

MÉTAIS, O., CHOLLET, J. P. & LESIEUR, M. 1983 Predictability of the large scales of freely-evolving three- and two-dimensional turbulence. In *Predictability of Fluid Motions. Proc. A.I.P. Conf.*, vol. 106, (ed. G. Holloway & B. J. West), pp. 303–319.

MÉTAIS, O. & LESIEUR, M. 1986 Statistical predictability of decaying turbulence. *J. Atmos. Sci.* **43**, 857–870.

METCALFE, R. W., ORSZAG, S. A., BRACHET, M. E., MENON, S. & RILEY, J. 1987 Secondary instability of a temporally growing mixing layer. *J. Fluid Mech.* **184**, 207–243.

MICHALKE, A. 1964 On the inviscid instability of the hyperbolic tangent velocity profile. *J. Fluid Mech.* **19**, 543–556.

MOFFATT, H. K. 1986 Geophysical and astrophysical turbulence. In *Proc. European Turbulence Conference, Lyon 1986* (ed. G. Comte-Bellot & J. Mathieu), pp. 228–244. Springer.

MOIN, M. & KIM, J. 1982 Numerical investigation of turbulent channel flow. *J. Fluid Mech.* **118**, 341–378.

MORY, M. & HOPFINGER, E. 1986 Structure functions in rotationally dominated turbulent flow. *Phys. Fluids* **29**, 2140–2146.

PEDLOSKY, J. 1979 *Geophysical Fluid Dynamics*. Springer.

PERRY, A. E. & CHONG, M. S. 1982 On the mechanism of wall turbulence. *J. Fluid Mech.* **119**, 173–217.

PERRY, A. E., CHONG, M. S. & LIM, T. T. 1982 Vortices in turbulence. In *Vortex motion, Proc. 75th Anniversary of the Aerodynamische Versuchsanstalt, Goettingen* (ed. H. G. Hornung & E. A. Muller), pp. 106–121. Friedr. Vieweg and Sohn.

PIERREHUMBERT, R. T. & WIDNALL, S. E. 1982 The two- and three-dimensional instabilities of a spatially periodic shear layer. *J. Fluid Mech.* **114**, 59–82.

RILEY, J. J. & METCALFE, R. W. 1980 Direct numerical simulation of a perturbed turbulent mixing layer. *AIAA 18th Aerospace Sci. Meeting, Pasadena*, 80-0274.

SCHWARZTRAUBER, P. & SWEET, R. 1980 Efficient fortran subprograms for the solution of EPD equations. *Rep. NCAR*. Boulder, Colorado.

SOMMERIA, J. 1986 Experimental study of the two-dimensional inverse energy cascade in a square box. *J. Fluid Mech.* **170**, 139–168.

STAQUET, C. 1985 Etude numérique de la transition à la turbulence bidimensionnelle dans une couche de mélange. Thèse de l'Université de Grenoble.

STAQUET, C., MÉTAIS, O. & LESIEUR, M. 1985 Etude de la couche de mélange et de sa cohérence du point de vue de la turbulence bidimensionnelle. *C.R. Acad. Sci., Paris* **300**, II, 833–838.

TANEDA, S. 1981 Large scale periodic motions in turbulent shear layers. *J. Phys. Soc. Japan* **50**, 1398–1403.

WINANT, C. D. & BROWAND, F. K. 1974 Vortex pairing: the mechanism of turbulent mixing layer growth at moderate Reynolds number. *J. Fluid Mech.* **63**, 237–255.

WOOD, D. H. & BRADSHAW, P. 1982 A turbulent mixing layer constrained by a solid wall. *J. Fluid Mech.* **122**, 57–90.

WYGNANSKI, I. & FIEDLER, H. E. 1970 The two-dimensional mixing region. *J. Fluid Mech.* **41**, 327–361.

ZABUSKY, N. J. & DEEM, G. S. 1971 Dynamical evolution of two-dimensional unstable shear flows. *J. Fluid Mech.* **47**, 353–379.